

**Two-pion exchange three-nucleon potential:  $\mathcal{O}(q^4)$  chiral expansion**S. Ishikawa<sup>1</sup> and M. R. Robilotta<sup>2</sup><sup>1</sup>*Department of Physics, Science Research Center, Hosei University, 2-17-1 Fujimi, Chiyoda, Tokyo 102-8160, Japan*<sup>2</sup>*Instituto de Física, Universidade de São Paulo, C.P. 66318, 05315-970, São Paulo, SP, Brazil*

(Received 3 April 2007; published 25 July 2007)

We present the expansion of the two-pion exchange three-nucleon potential (TPE-3NP) to chiral order  $q^4$ , which corresponds to a subset of all possibilities at this order and is based on the  $\pi N$  amplitude at  $\mathcal{O}(q^3)$ . Results encompass both numerical corrections to strength coefficients of previous  $\mathcal{O}(q^3)$  terms and new structures in the profile functions. The former are typically smaller than 10% whereas the latter arise from either loop functions or nonlocal gradients acting on the wave function. The influence of the new TPE-3NP over static and scattering three-body observables has been assessed and found to be small, as expected from perturbative corrections.

DOI: [10.1103/PhysRevC.76.014006](https://doi.org/10.1103/PhysRevC.76.014006)

PACS number(s): 21.30.Fe, 13.75.Cs, 13.75.Gx

**I. INTRODUCTION**

The research program for nuclear forces, outlined more than fifty years ago by Taketani, Nakamura, and Sasaki [1], treats pions and nucleons as basic degrees of freedom. This insight proved to be very fruitful. On the one hand, it implies the interconnection of all nuclear processes, both among themselves and with a class of free reactions. On the other, it determines a close relationship between the number  $\mathcal{N}_\pi$  of pions involved in a given interaction and its range  $r$ , which can be roughly summarized by the factor  $Y^{\mathcal{N}_\pi}$ , where  $Y = e^{-\mu r}/r$  is the Yukawa function and  $\mu$  is the pion mass. As a consequence, the outer components of nuclear forces are dominated by just a few basic subamplitudes, describing either single ( $N \rightarrow \pi N$ ) or multipion ( $\pi\pi \rightarrow \pi\pi$ ,  $\pi N \rightarrow \pi N$ ,  $\pi N \rightarrow \pi\pi N$ , ...) interactions.

It took a long time before a theoretical tool became available that allows the precise treatment of these amplitudes. Nowadays, owing to the development of chiral perturbation theory (ChPT) in association with effective Lagrangians [2,3], the roles of pions and nucleons in nuclear forces can be described consistently. The rationale for this approach is that the quarks  $u$  and  $d$ , which have small masses, dominate low-energy interactions. One then works with a two-flavor version of QCD and treats their masses as perturbations in a chiral symmetric Lagrangian. The systematic inclusion of quark mass contributions is performed by means of chiral perturbation theory, which incorporates low-energy features of QCD into the nuclear force problem. In performing perturbative expansions, one uses a typical scale  $q$ , set by either pion four-momenta or nucleon three-momenta, such that  $q \ll 1$  GeV.

Range and chiral expansions are not mutually exclusive and, in fact, the joint application of both approaches to nuclear systems has promoted a considerable refinement in the description of their interactions in the past decade. The one-pion exchange potential (OPEP) corresponds to  $\mathcal{N}_\pi = 1$ , begins [4] at  $\mathcal{O}(q^0)$ , and fortunately is the leading term in both approaches. This component provides a good description of  $NN$  interactions at large distances and became well established in the 1960s. The next class of two-body contributions is associated with exchanges of two uncorrelated pions, with

$\mathcal{N}_\pi = 2$ . As far as chiral symmetry is concerned, the two-pion exchange potential (TPEP) begins at  $\mathcal{O}(q^2)$  and, at present, there are two independent expansions up to  $\mathcal{O}(q^4)$  in the literature, based on either heavy-baryon [5] or covariant [6,7] ChPT. The TPEP is closely related with the off-shell  $\pi N$  amplitude and, at this order, two-loop diagrams involving intermediate  $\pi\pi$  scattering already begin to contribute. At present, the OPEP and the TPEP are the only components of the two-body force understood in some depth. Exploratory works for processes involving the exchange of three pions exist [8], but much more research is needed before a reliable picture can be produced. In the absence of a comprehensive theoretical description, phenomenological form factors taken from phase shifts and the deuteron binding energy are still required [9] in the region  $r < 1$  fm.

In proper three-nucleon ( $3N$ ) interactions, the leading term corresponds to the two-pion exchange three-nucleon potential TPE-3NP, in which the pion emitted by a nucleon is scattered before being absorbed by another one. It has  $\mathcal{N}_\pi = 2$  in the range expansion and the earliest version was produced exactly fifty years by Fujita and Miyazawa [10]. In the chiral expansion, this contribution begins at  $\mathcal{O}(q^3)$ , and formulations at this order, which involve only tree-level interactions, have been available for a long time [11–13]. In this work we consider the extension of the three-nucleon force to  $\mathcal{O}(q^4)$ , so as to achieve consistency with the available  $NN$  picture. However, the implementation of this program is not straightforward, since it requires the evaluation of a rather large number of diagrams, encompassing ranges with  $\mathcal{N}_\pi = 2$  and  $\mathcal{N}_\pi = 3$ . With the purpose of exploring the magnitude of  $\mathcal{O}(q^4)$  effects, in this work we concentrate on the particular subset of processes pertaining to the former case, which still belong to the TPE-3NP class.

Our presentation is divided as follows. In Sec. II we display the general relationship between the TPE-3NP and the  $\pi N$  amplitude to discuss how it affects chiral power counting in the former. The  $\pi N$  amplitude relevant for the  $\mathcal{O}(q^4)$  potential is derived in Sec. III and used to construct the three-body interaction in Sec. IV. We concentrate on numerical changes induced into both potential parameters and observables in Secs. V and VI, and conclusions are presented in Sec. VII.

There are also four appendices, dealing with kinematics,  $\pi N$  subthreshold coefficients, loop integrals, and nonlocal terms.

## II. GENERAL FORMULATION

Potentials to be used into nonrelativistic equations can be derived from field theory by means of the  $T$  matrix. In the case of three-nucleon potentials, one starts from the nonrelativistic transition matrix describing the process  $N(p_1)N(p_2)N(p_3) \rightarrow N(p'_1)N(p'_2)N(p'_3)$ , which includes both kernels and their iterations. The former correspond to proper interactions, represented by diagrams that cannot be split into two pieces by cutting positive-energy nucleon lines only, whereas the latter are automatically generated by the dynamical equation. Therefore, just the kernels, denoted collectively by  $\bar{t}_3$ , are included in the potential.

The transformation of a  $T$  matrix into a potential depends on both the dynamical equation adopted and conventions associated with off-shell effects. The latter were discussed in a comprehensive paper by Friar [14]. Here we use the kinematical variables defined in Appendix A and relate  $\bar{t}_3$  to the momentum-space potential operator  $\hat{W}$  by writing [15]

$$\langle \mathbf{p}'_1, \mathbf{p}'_2, \mathbf{p}'_3 | \hat{W} | \mathbf{p}_1, \mathbf{p}_2, \mathbf{p}_3 \rangle = -(2\pi)^3 \delta^3(\mathbf{P}' - \mathbf{P}) \bar{t}_3(\mathbf{p}'_1, \mathbf{p}'_2, \mathbf{p}'_3, \mathbf{p}_1, \mathbf{p}_2, \mathbf{p}_3). \quad (1)$$

In configuration space, internal dynamics is described by the function

$$\begin{aligned} W(\mathbf{r}', \boldsymbol{\rho}'; \mathbf{r}, \boldsymbol{\rho}) &= -[2/\sqrt{3}]^6 \int \frac{d\mathbf{Q}_r}{(2\pi)^3} \frac{d\mathbf{Q}_\rho}{(2\pi)^3} \frac{d\mathbf{q}_r}{(2\pi)^3} \frac{d\mathbf{q}_\rho}{(2\pi)^3} \\ &\times e^{i[\mathbf{Q}_r \cdot (\mathbf{r}' - \mathbf{r}) + \mathbf{Q}_\rho \cdot (\boldsymbol{\rho}' - \boldsymbol{\rho}) + \mathbf{q}_r \cdot (\mathbf{r}' + \mathbf{r})/2 + \mathbf{q}_\rho \cdot (\boldsymbol{\rho}' + \boldsymbol{\rho})/2]} \\ &\times \bar{t}_3(\mathbf{Q}_r, \mathbf{Q}_\rho, \mathbf{q}_r, \mathbf{q}_\rho), \end{aligned} \quad (2)$$

which is to be used in a nonlocal version of the Schrödinger equation:

$$\begin{aligned} \left[ -\frac{1}{m} \nabla_{r'}^2 - \frac{1}{m} \nabla_{\rho'}^2 - \epsilon \right] \psi(\mathbf{r}', \boldsymbol{\rho}') \\ = -[\sqrt{3}/2]^3 \int d\mathbf{r} d\boldsymbol{\rho} W(\mathbf{r}', \boldsymbol{\rho}'; \mathbf{r}, \boldsymbol{\rho}) \psi(\mathbf{r}, \boldsymbol{\rho}). \end{aligned} \quad (3)$$

Nonlocal effects are associated with the variables  $\mathbf{Q}_r$  and  $\mathbf{Q}_\rho$ . When these effects are not too strong, they can be represented by gradients acting on the wave function and the potential  $W$  is rewritten as

$$W(\mathbf{r}', \boldsymbol{\rho}'; \mathbf{r}, \boldsymbol{\rho}) = \delta^3(\mathbf{r}' - \mathbf{r}) \delta^3(\boldsymbol{\rho}' - \boldsymbol{\rho}) [2/\sqrt{3}]^3 V(\mathbf{r}, \boldsymbol{\rho}). \quad (4)$$

The two-pion exchange three-nucleon potential is represented in Fig. 1(a). It is closely related with the  $\pi N$  scattering amplitude, which is  $\mathcal{O}(q)$  for free pions and becomes  $\mathcal{O}(q^2)$  within the three-nucleon system. As a consequence, the TPE-3NP begins at  $\mathcal{O}(q^3)$  and, at this order, it also receives contributions from interactions (c) and (d), which have shorter range. The extension of the chiral series to  $\mathcal{O}(q^4)$  requires both the inclusion of single-loop effects into processes that already contribute at  $\mathcal{O}(q^3)$  and the evaluation of many new amplitudes, especially those associated with diagram (b).

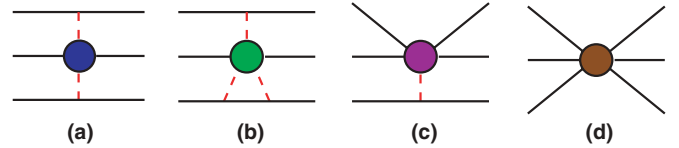


FIG. 1. (Color online) Classes of three-nucleon forces, where full and dashed lines represent nucleons and pions, respectively; diagram (a) corresponds to the TPE-3NP.

In this paper we concentrate on the particular set of processes that belong to the TPE-3NP class, represented by the  $T$  matrix  $\mathcal{T}_{\pi\pi}$  and evaluated by using the kinematical conditions given in Fig. 2. The coupling of a pion to nucleon  $i = (1, 2)$  is derived from the usual lowest order pseudo-vector Lagrangian  $\mathcal{L}^{(1)}$  and the Dirac equation yields the equivalent forms for the vertex

$$(g_A/2f_\pi)[\tau \bar{u}(p' - p)\gamma_5 u]^{(i)} = (mg_A/f_\pi)[\tau \bar{u}\gamma_5 u]^{(i)}, \quad (5)$$

where  $g_A$ ,  $f_\pi$ , and  $m$  represent, respectively, the axial nucleon decay, the pion decay, and the nucleon mass.

The amplitude for the intermediate process  $\pi^a(k)N(p) \rightarrow \pi^b(k')N(p')$  has the isospin structure

$$T_{ba} = \delta_{ab} T^+ + i\epsilon_{bac} \tau_c T^- \quad (6)$$

and Fig. 2 yields

$$\begin{aligned} \mathcal{T}_{\pi\pi} = - \left[ \frac{mg_A}{f_\pi} \right]^2 [\bar{u}\gamma_5 u]^{(1)} [\bar{u}\gamma_5 u]^{(2)} \frac{1}{k^2 - \mu^2} \frac{1}{k'^2 - \mu^2} \\ [\boldsymbol{\tau}^{(1)} \cdot \boldsymbol{\tau}^{(2)} T^+ - i\boldsymbol{\tau}^{(1)} \times \boldsymbol{\tau}^{(2)} \cdot \boldsymbol{\tau}^{(3)} T^-]^{(3)}. \end{aligned} \quad (7)$$

The results in Appendix A show that  $[\bar{u}\gamma_5 u]^{(i)} \rightarrow \mathcal{O}(q)$ , whereas pion propagators are  $\mathcal{O}(q^{-2})$ . As a consequence, in the  $\mathcal{O}(q^4)$  expansion of the potential one needs  $\mathcal{T}_{\pi\pi}$  to  $\mathcal{O}(q)$  and  $T^\pm$  to  $\mathcal{O}(q^3)$ . For on-shell nucleons, the subamplitudes  $T^\pm$  can be written as

$$T^\pm = \bar{u}(p') \left[ D^\pm - \frac{i}{2m} \sigma_{\mu\nu} (p' - p)^\mu K^\nu B^\pm \right] u(p), \quad (8)$$

with  $K = (k' + k)/2$ . The dynamical content of the  $\pi N$  interaction is carried by the functions  $D^\pm$  and  $B^\pm$  and their main properties were reviewed by Höhler [16]. The chiral structure of these subamplitudes was discussed by Becher and Leutwyler [17,18] a few years ago, in the framework of covariant perturbation theory, and here we employ their results. As far as power counting is concerned, in Appendix A

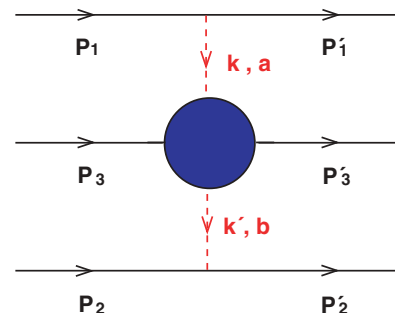


FIG. 2. (Color online) Two-pion exchange three-nucleon potential.

one finds  $[\bar{u}(\mathbf{p}')u(\mathbf{p})]^{(3)} \rightarrow \mathcal{O}(q^0)$  and  $[\frac{i}{2m}\bar{u}(\mathbf{p}')\sigma_{\mu\nu}(p' - p)^\mu K^\nu u(\mathbf{p})]^{(3)} \rightarrow \mathcal{O}(q^2)$ , indicating that one needs the expansions of  $D^\pm$  and  $B^\pm$  up to  $\mathcal{O}(q^3)$  and  $\mathcal{O}(q)$ , respectively.

At low and intermediate energies, the  $\pi N$  amplitude is given by a nucleon pole superimposed on a smooth background. One then distinguishes the pseudovector (PV) Born term from a remainder (R) and writes

$$T^\pm = T_{pv}^\pm + T_R^\pm. \quad (9)$$

The former contribution depends on just two observables, namely the nucleon mass  $m$  and the  $\pi N$  coupling constant  $g$ , as prescribed by the Ward-Takahashi identity [19]. The calculation of these quantities in ChPT may involve loops and other coupling constants but, at the end, results must be organized so as to reproduce the physical values of both  $m$  and  $g$  in  $T_{pv}^\pm$  [20]. For this reason, one uses the constant  $g$ , instead of  $(g_A/f_\pi)$ , since the former is indeed the observable determined by the residue of the nucleon pole [16,18,21]. The  $pv$  Born subamplitudes are given by

$$D_{pv}^+ = \frac{g^2}{2m} \left( \frac{k' \cdot k}{s - m^2} + \frac{k' \cdot k}{u - m^2} \right), \quad (10)$$

$$B_{pv}^+ = -g^2 \left( \frac{1}{s - m^2} - \frac{1}{u - m^2} \right), \quad (11)$$

$$D_{pv}^- = \frac{g^2}{2m} \left( \frac{k \cdot k'}{s - m^2} - \frac{k \cdot k'}{u - m^2} - \frac{v}{m} \right), \quad (12)$$

$$B_{pv}^- = -g^2 \left( \frac{1}{s - m^2} + \frac{1}{u - m^2} + \frac{1}{2m^2} \right), \quad (13)$$

where  $s$  and  $u$  are the usual  $\pi N$  Mandelstam variables. In the case of free pions, their chiral orders are, respectively,  $[D_{pv}^+, B_{pv}^+, D_{pv}^-, B_{pv}^-] \rightarrow \mathcal{O}[q^2, q^{-1}, q, q^0]$ , but important changes do occur when the pions become off-shell.

The amplitudes  $T_R^\pm$  receive contributions from both tree interactions and loops. The former can be read directly from the basic Lagrangians and correspond to polynomials in  $t = (k' - k)^2$  and  $v = (p' + p) \cdot (k' + k)/4m$ , with coefficients given by renormalized low energy constants (LECs) [18]. The latter are more complex and depend on Feynman integrals. In the description of  $\pi N$  amplitudes below threshold, one approximates both types of contributions by polynomials and writes [16,22]

$$X_R = \sum x_{mn} v^{2m} t^n, \quad (14)$$

where  $X_R$  stands for  $D_R^+$ ,  $B_R^+/\nu$ ,  $D_R^-/\nu$ , or  $B_R^-$ . The subthreshold coefficients  $x_{mn}$  have the status of observables, since they can be obtained by means of dispersion relations applied to scattering data. As such, they constitute an important source of information about the values of the LECs to be used in effective Lagrangians. The dynamical role of a given subthreshold coefficient depends on whether the pions involved in the  $\pi N$  amplitude are free or virtual. In the former case, one has  $\nu \rightarrow \mathcal{O}(q)$ , whereas in the TPE-3NP,  $\nu \rightarrow \mathcal{O}(q^2)$ , as shown in Appendix A.

The isospin-odd subthreshold coefficients include leading order terms, which implement the predictions made by Weinberg [23] and Tomozawa [24] for  $\pi N$  scattering lengths,

given by

$$D_{WT}^- = \frac{\nu}{2f_\pi^2}, \quad B_{WT}^- = \frac{1}{2f_\pi^2}. \quad (15)$$

For free pions, one has  $[D_{WT}^-, B_{WT}^-] \rightarrow \mathcal{O}[q, q^0]$  and these orders of magnitude also change when pions become virtual.

Quite generally, the ranges of nuclear interactions are determined by  $t$ -channel exchanges. At  $\mathcal{O}(q^3)$ , the TPE-3NP involves only single-pion exchanges among different nucleons and has the longest possible range. Another  $t$ -channel structure, associated with the pion cloud of the nucleon, becomes apparent at  $\mathcal{O}(q^4)$  and gives rise to both scalar and vector form factors [21]. These effects extend well beyond 1 fm [25,26] and a limitation of the power series given by Eq. (14) is that they cannot accommodate these ranges, since Fourier transforms of polynomials yield only  $\delta$  functions and their derivatives. In the description of the  $\pi N$  amplitude produced by Becher and Leutwyler [18], one learns that the only sources of medium-range ( $mr$ ) effects are their diagrams  $k$  and  $l$ , which contain two pions propagating in the  $t$  channel. In our derivation of the TPE-3NP, the loop content of these diagrams is not approximated by power series and, for free pions, the nonpole subamplitudes are written as

$$D_R^+ = D_{mr}^+(t) + [\bar{d}_{00}^+ + d_{10}^+ v^2 + \bar{d}_{01}^+ t]_{(2)} + [d_{20}^+ v^4 + d_{11}^+ v^2 t + \bar{d}_{02}^+ t^2]_{(3)}, \quad (16)$$

$$B_R^+ = B_{mr}^+(t) + [b_{00}^+ v]_{(1)}, \quad (17)$$

$$D_R^- = D_{mr}^-(t) + [\nu/(2f_\pi^2)]_{(1)} + [\bar{d}_{00}^- \nu + d_{10}^- v^3 + \bar{d}_{01}^- \nu t]_{(3)}, \quad (18)$$

$$B_R^- = B_{mr}^-(t) + [1/(2f_\pi^2) + \bar{b}_{00}^-]_{(0)} + [b_{10}^- v^2 + \bar{b}_{01}^- t]_{(1)}, \quad (19)$$

where the labels ( $n$ ) outside the brackets indicate the presence of  $\mathcal{O}(q^n)$  leading terms and  $mr$  denotes terms associated with the nucleon pion cloud. The  $\bar{\phantom{x}}$  symbol over some coefficients indicates that they do not include both Weinberg-Tomozawa and medium-range contributions, which are accounted for explicitly. The functions  $D_R^\pm$  and  $B_R^\pm$  depend on the parameters  $f_\pi$ ,  $g_A$ ,  $\mu$ , and  $m$  and on the LECs  $c_i$  and  $\bar{d}_i$ , which appear into higher order terms of the effective Lagrangian. The subthreshold coefficients are the door through which LECs enter our calculation and their explicit forms are given in Appendix B.

The dynamical content of the  $\mathcal{O}(q^3)$   $\pi N$  amplitude is shown in Fig. 3. The first two diagrams correspond to PV Born amplitudes, whereas the third one represents the Weinberg-Tomozawa contact interaction, all of them with physical masses and coupling constants. The fourth graph summarizes the terms within square brackets in Eqs. (16)–(19) and depends on the LECs. Finally, the last two diagrams describe medium-range effects owing to the nucleon pion cloud, associated with scalar and vector form factors. This decomposition of the  $\pi N$  amplitude has also been used in our derivation of the two-pion exchange components of the  $NN$  interaction [6,7] and hence the present calculation is consistent with those results.

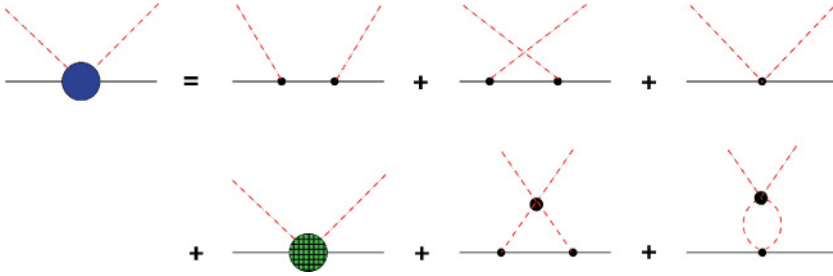


FIG. 3. (Color online) Representation of the  $\pi N$  amplitude used in the construction of the TPE-3NP.

### III. INTERMEDIATE $\pi N$ AMPLITUDE

The combination of Figs. 2 and 3 gives rise to the TPE-3NP, associated with the six diagrams shown in Fig. 4. In the sequence, we discuss their individual contributions to the subamplitudes  $D^\pm$  and  $B^\pm$ . We are interested only in the longest possible component of the potential, and numerators of expressions are systematically simplified by using  $k^2 \rightarrow \mu^2$  and  $k'^2 \rightarrow \mu^2$ . In configuration space, this corresponds to keeping only those terms that contain two Yukawa functions and neglecting interactions associated with Figs. 1(c) and 1(d).

#### A. Diagrams (a) and (b)

The crosses in the nucleon propagators of Figs. 4(a) and 4(b) indicate that they do not include forward-propagating components, so as to avoid double counting when the potential is used in the dynamical equation. The covariant evaluation of these contributions is based on Eqs. (10)–(13). Denoting by  $\bar{p}$  the momenta of the propagating nucleons, one decomposes the factors  $1/(s - m^2)$  and  $1/(u - m^2)$  as

$$\frac{1}{(\bar{p}^0)^2 - \bar{E}^2} = \frac{1}{2\bar{E}(\bar{p}^0 - \bar{E})} - \frac{1}{2\bar{E}(\bar{p}^0 + \bar{E})}, \quad (20)$$

with  $\bar{E} = \sqrt{m^2 + \bar{p}^2}$ . The first term represents forward-propagating nucleons, associated with the iteration of the OPEP, whereas the second one gives rise to connected contributions. Discarding the former and using the results of Appendix A, one has

$$\frac{1}{(s_u - m^2)} \rightarrow -1/[4m^2 + (3q_r^2 + q_\rho^2/3 + 16Q_\rho^2/3 \pm 10q_r \cdot Q_\rho/\sqrt{3} \mp 2q_\rho \cdot Q_r/\sqrt{3})]. \quad (21)$$

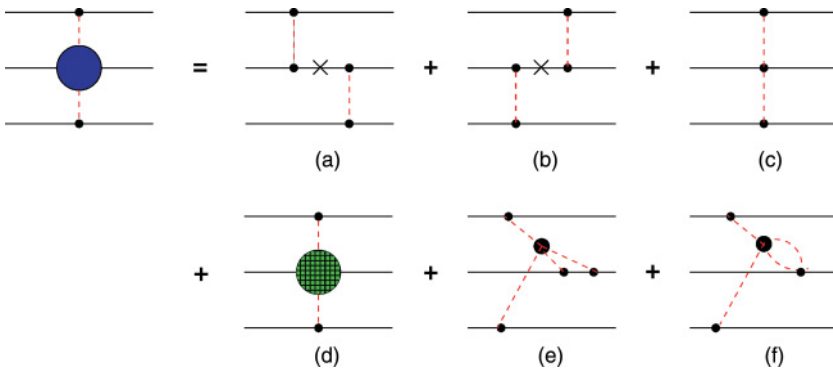


FIG. 4. (Color online) Structure of the  $\mathcal{O}(q^4)$  two-pion exchange three-nucleon potential.

After appropriate truncation, one obtains

$$D_{ab}^+ = -\frac{g^2}{8m^3}(2\mu^2 - t) \rightarrow \mathcal{O}(q^2), \quad (22)$$

$$B_{ab}^+ \rightarrow \mathcal{O}(q^2), \quad (23)$$

$$D_{ab}^- = -\frac{g^2}{2m^2}\nu \rightarrow \mathcal{O}(q^2), \quad (24)$$

$$B_{ab}^- \rightarrow \mathcal{O}(q^2), \quad (25)$$

where we have used the fact that, in the case of virtual pions,  $\nu \rightarrow \mathcal{O}(q^2)$ .

#### B. Diagrams (c) and (d)

These contributions are purely polynomial, can be read directly from Eqs. (16)–(19), and are given by

$$D_{cd}^+ = -\frac{4c_1}{f_\pi^2}\mu^2 + \left[ \frac{c_3}{f_\pi^2} + \frac{g_A^4\mu}{16\pi f_\pi^4} \right] (2\mu^2 - t) \rightarrow \mathcal{O}(q^2), \quad (26)$$

$$B_{cd}^+ \rightarrow \mathcal{O}(q^2), \quad (27)$$

$$D_{cd}^- = \frac{1}{2f_\pi^2}\nu \rightarrow \mathcal{O}(q^2), \quad (28)$$

$$B_{cd}^- = \frac{1}{2f_\pi^2} + \frac{2c_4m}{f_\pi^2} - \frac{g_A^4m\mu}{8\pi f_\pi^4} \rightarrow \mathcal{O}(q^0). \quad (29)$$

#### C. Diagrams (e) and (f)

The medium-range components of the intermediate  $\pi N$  amplitude are

$$D_e^+ = \frac{g_A^2\mu}{64\pi^2 f_\pi^4} (2t - \mu^2) [(1 - t/2\mu^2)\Pi_t - 2\pi] \rightarrow \mathcal{O}(q^3), \quad (30)$$

$$D_{ef}^+ \rightarrow \mathcal{O}(q^4), \quad (31)$$

$$B_e^- = \frac{g_A^2 m \mu}{16\pi^2 f_\pi^4} [(1 - t/4\mu^2)\Pi_t - \pi] \rightarrow \mathcal{O}(q), \quad (32)$$

where  $\Pi_t$  is the dimensionless Feynman integral

$$\begin{aligned} \Pi_t &= \int_0^1 da \frac{\mu^2 F(a)}{t - M^2} \leftarrow M = 2\mu/a, \\ F(a) &= \frac{8}{a^2} \tan^{-1} \left[ \frac{ma\sqrt{1-a^2}}{\mu(1-a^2/2)} \right]. \end{aligned} \quad (33)$$

The amplitude  $D_{ef}^-$ , proportional to  $v$ , is  $\mathcal{O}(q^3)$  for free pions and here becomes  $\mathcal{O}(q^4)$ . Thus, in fact, diagram (f) does not contribute to the TPE-3NP at  $\mathcal{O}(q^4)$ .

#### D. Full results

The Golberger-Treiman relation  $g/m = g_A/f_\pi$  is valid up to  $\mathcal{O}(q^2)$  and can be used in diagrams (a) and (b). One then has

$$\begin{aligned} D^+ &= \frac{\sigma(2\mu^2)}{f_\pi^2} + \frac{(2\mu^2 - t)}{f_\pi^2} \left[ -\frac{g_A^2}{8m} + c_3 + \frac{g_A^2(1 + g_A^2)\mu}{16\pi f_\pi^2} \right. \\ &\quad \left. - \frac{g_A^2 \mu}{128\pi^2 f_\pi^2} (1 - 2t/\mu^2)\Pi_t \right], \end{aligned} \quad (34)$$

where

$$\sigma(t = 2\mu^2) = -4c_1\mu^2 - \frac{3g_A^2\mu^3}{32\pi f_\pi^2} \quad (35)$$

is the value of the scalar form factor at the Cheng-Dashen point [17]. The remaining amplitudes read

$$B^+ \rightarrow \mathcal{O}(q^2), \quad (36)$$

$$D^- = \frac{1 - g_A^2}{2f_\pi^2} v, \quad (37)$$

$$\begin{aligned} B^- &= \frac{1 + 4c_4 m}{2f_\pi^2} - \frac{g_A^2(1 + 2g_A^2)m\mu}{16\pi f_\pi^4} \\ &\quad + \frac{g_A^2 m \mu}{16\pi^2 f_\pi^4} (1 - t/4\mu^2)\Pi_t. \end{aligned} \quad (38)$$

The subamplitudes  $D^\pm$  and  $B^\pm$  begin at  $\mathcal{O}(q^2)$  and one needs just the leading terms in the spinor matrix elements of Eq. (8), which is rewritten as

$$T^+ = 2mD^+, \quad (39)$$

$$T^- = 2mD^- + i\boldsymbol{\sigma}^{(3)} \cdot \mathbf{k}' \times \mathbf{k}B^-, \quad (40)$$

with  $D^+ \rightarrow \mathcal{O}(q^2) + \mathcal{O}(q^3)$ ,  $D^- \rightarrow \mathcal{O}(q^2)$ , and  $B^- \rightarrow \mathcal{O}(q^0) + \mathcal{O}(q)$ .

#### E. $\mathcal{O}(q^3)$ reduction

To compare our amplitudes with previous  $\mathcal{O}(q^3)$  results, one notes that, in case corrections are dropped, one

would have

$$D^+ = \frac{\sigma(0)}{f_\pi^2} + \frac{(2\mu^2 - t)}{f_\pi^2} \left\{ -\left[ \frac{g_A^2}{8m} \right] + c_3 \right\}, \quad (41)$$

$$B^- = \left[ \frac{1}{2f_\pi^2} \right] + \frac{2c_4 m}{f_\pi^2}. \quad (42)$$

These expressions agree with those derived directly from a chiral Lagrangian [27], except for the terms within square brackets in both  $D^+$  and  $B^-$ . The former corresponds to a Born contribution whereas the latter is due to diagram (c) in Fig. 4, associated with the Weinberg-Tomozawa term.

#### IV. TWO-PION EXCHANGE POTENTIAL

The expansion of the TPE-3NP up to  $\mathcal{O}(q^4)$  requires only leading terms in vertices and propagators. To derive the nonrelativistic potential in momentum space, one divides Eq. (7) by the relativistic normalization factor  $\sqrt{2E} \simeq \sqrt{2m}$  for each external nucleon leg and writes<sup>1</sup>

$$\begin{aligned} \bar{t}_3 &= \frac{g_A^2}{4f_\pi^2} \frac{1}{\mathbf{k}^2 + \mu^2} \frac{1}{\mathbf{k}'^2 + \mu^2} \boldsymbol{\sigma}^{(1)} \cdot \mathbf{k} \boldsymbol{\sigma}^{(2)} \cdot \mathbf{k}' \\ &\quad \times \left[ \boldsymbol{\tau}^{(1)} \cdot \boldsymbol{\tau}^{(2)} D^+ - i \boldsymbol{\tau}^{(1)} \times \boldsymbol{\tau}^{(2)} \cdot \boldsymbol{\tau}^{(3)} \right. \\ &\quad \left. \times \left( D^- + \frac{i}{2m} \boldsymbol{\sigma}^{(3)} \cdot \mathbf{k}' \times \mathbf{k} B^- \right) \right]. \end{aligned} \quad (43)$$

The configuration space potential has the form

$$\begin{aligned} V_3(\mathbf{r}, \boldsymbol{\rho}) &= \boldsymbol{\tau}^{(1)} \cdot \boldsymbol{\tau}^{(2)} V_3^+(\mathbf{r}, \boldsymbol{\rho}) + \boldsymbol{\tau}^{(1)} \times \boldsymbol{\tau}^{(2)} \cdot \boldsymbol{\tau}^{(3)} V_3^-(\mathbf{r}, \boldsymbol{\rho}) \\ &\quad + \text{cyclic permutations}, \end{aligned} \quad (44)$$

with

$$\begin{aligned} V_3^+(\mathbf{r}, \boldsymbol{\rho}) &= C_1^+ \boldsymbol{\sigma}^{(1)} \cdot \hat{\mathbf{x}}_{31} \boldsymbol{\sigma}^{(2)} \cdot \hat{\mathbf{x}}_{23} U_1(x_{31}) U_1(x_{23}) \\ &\quad + C_2^+ \{ (1/9) \boldsymbol{\sigma}^{(1)} \cdot \boldsymbol{\sigma}^{(2)} [U(x_{31}) - U_2(x_{31})] \\ &\quad \times [U(x_{23}) - U_2(x_{23})] + (1/3) \boldsymbol{\sigma}^{(1)} \cdot \hat{\mathbf{x}}_{23} \boldsymbol{\sigma}^{(2)} \cdot \hat{\mathbf{x}}_{23} \\ &\quad \times [U(x_{31}) - U_2(x_{31})] U_2(x_{23}) + (1/3) \boldsymbol{\sigma}^{(1)} \cdot \hat{\mathbf{x}}_{31} \\ &\quad \times \boldsymbol{\sigma}^{(2)} \cdot \hat{\mathbf{x}}_{31} U_2(x_{31}) [U(x_{23}) - U_2(x_{23})] \\ &\quad + \boldsymbol{\sigma}^{(1)} \cdot \hat{\mathbf{x}}_{31} \boldsymbol{\sigma}^{(2)} \cdot \hat{\mathbf{x}}_{23} \hat{\mathbf{x}}_{31} \cdot \hat{\mathbf{x}}_{23} U_2(x_{31}) U_2(x_{23}) \} \\ &\quad + C_3^+ \boldsymbol{\sigma}^{(1)} \cdot \nabla_{31}^l \boldsymbol{\sigma}^{(2)} \cdot \nabla_{23}^l \nabla_{31}^l \cdot \nabla_{23}^l [I^0 - 2I^1], \end{aligned} \quad (45)$$

$$\begin{aligned} V_3^-(\mathbf{r}, \boldsymbol{\rho}) &= C_1^- \{ (1/9) \boldsymbol{\sigma}^{(1)} \times \boldsymbol{\sigma}^{(2)} \cdot \boldsymbol{\sigma}^{(3)} [U(x_{31}) - U_2(x_{31})] \\ &\quad \times [U(x_{23}) - U_2(x_{23})] + (1/3) \boldsymbol{\sigma}^{(3)} \times \boldsymbol{\sigma}^{(1)} \cdot \hat{\mathbf{x}}_{23} \boldsymbol{\sigma}^{(2)} \cdot \hat{\mathbf{x}}_{23} \\ &\quad \times [U(x_{31}) - U_2(x_{31})] U(x_{23}) + (1/3) \boldsymbol{\sigma}^{(1)} \cdot \hat{\mathbf{x}}_{31} \boldsymbol{\sigma}^{(2)} \\ &\quad \times \boldsymbol{\sigma}^{(3)} \cdot \hat{\mathbf{x}}_{31} U_2(x_{31}) [U(x_{23}) - U_2(x_{23})] + \boldsymbol{\sigma}^{(1)} \cdot \hat{\mathbf{x}}_{31} \boldsymbol{\sigma}^{(2)} \\ &\quad \cdot \hat{\mathbf{x}}_{23} \boldsymbol{\sigma}^{(3)} \cdot \hat{\mathbf{x}}_{31} \hat{\mathbf{x}}_{23} U_2(x_{31}) U_2(x_{23}) \} \\ &\quad + C_2^- \{ \boldsymbol{\sigma}^{(1)} \cdot (i \nabla_{31}^{wf} - i \nabla_{23}^{wf}) \boldsymbol{\sigma}^{(2)} \cdot \hat{\mathbf{x}}_{23} [U(x_{31}) \\ &\quad - U_2(x_{31})] U_1(x_{23}) + \boldsymbol{\sigma}^{(1)} \cdot \hat{\mathbf{x}}_{31} \boldsymbol{\sigma}^{(2)} \cdot (i \nabla_{31}^{wf} - i \nabla_{23}^{wf}) \end{aligned}$$

<sup>1</sup>One notes that this expression is identical with Eq. (33) of Ref. [13] divided by  $8m^3$ .

$$\begin{aligned}
& \times U_1(x_{31})[U(x_{23}) - U_2(x_{23})] + 3\sigma^{(1)} \cdot \hat{x}_{31}\sigma^{(2)} \cdot \hat{x}_{23} \\
& \times (i\nabla_{31}^{wf} - i\nabla_{23}^{wf}) \cdot [\hat{x}_{31}U_2(x_{31})U_1(x_{23}) \\
& + \hat{x}_{23}U_1(x_{31})U_2(x_{23})] \} + C_3^- \sigma^{(1)} \cdot \nabla_{31}^I \sigma^{(2)} \cdot \nabla_{23}^I \sigma^{(3)} \\
& \cdot \nabla_{31}^I \times \nabla_{23}^I [I^0 - I^1/4]. \quad (46)
\end{aligned}$$

The profile functions are written in terms of the dimensionless variables  $x_{ij} = \mu x_{ij}$  and read

$$U(x) = \frac{e^{-x}}{x}, \quad (47)$$

$$U_1(x) = -\left(1 + \frac{1}{x}\right) \frac{e^{-x}}{x}, \quad (48)$$

$$U_2(x) = \left(1 + \frac{3}{x} + \frac{3}{x^2}\right) \frac{e^{-x}}{x}, \quad (49)$$

$$\begin{aligned}
I^n &= -\frac{16\pi}{\mu^2} \int \frac{dk}{(2\pi)^3} \frac{dk'}{(2\pi)^3} e^{i(k \cdot r_{31} + k' \cdot r_{23})} \left[ \frac{t}{\mu^2} \right]^n \\
&\times \frac{1}{k^2 + \mu^2} \frac{1}{k'^2 + \mu^2} \Pi_t(t). \quad (50)
\end{aligned}$$

The last function involves the loop integral given in Eq. (33) and is discussed further in Appendix C. The gradients  $\nabla_{ij}^I$  act on the functions  $I^n$ , whereas the  $\nabla_{ij}^{wf}$  act *only* on the wave function and give rise to nonlocal interactions, as discussed in Appendix D.

The strength coefficients are the following combinations of the basic coupling constants:

$$C_1^+ = \frac{g_A^2 \mu^4}{64\pi^2 f_\pi^4} \sigma(2\mu^2), \quad (51)$$

$$C_2^+ = \frac{g_A^2 \mu^6}{32\pi^2 f_\pi^4 m} \left( -\frac{g_A^2}{8} + mc_3 + \frac{g_A^2(1 + g_A^2)m\mu}{16\pi f_\pi^2} \right), \quad (52)$$

$$C_3^+ = \frac{g_A^4 \mu^7}{4096\pi^3 f_\pi^6}, \quad (53)$$

$$C_1^- = \frac{g_A^2 \mu^6}{256\pi^2 f_\pi^4 m} \left( 1 + 4mc_4 - \frac{g_A^2(1 + 2g_A^2)m\mu}{8\pi f_\pi^2} \right), \quad (54)$$

$$C_2^- = \frac{g_A^2 (g_A^2 - 1) \mu^6}{768\pi^2 f_\pi^4 m}, \quad (55)$$

$$C_3^- = -\frac{g_A^4 \mu^7}{2048\pi^3 f_\pi^6}. \quad (56)$$

## V. STRENGTH COEFFICIENTS

The strength constants of the potential involve a blend of four well-determined parameters, namely  $m = 938.28$  MeV,  $\mu = 139.57$  MeV,  $g_A = 1.267$ , and  $f_\pi = 92.4$  MeV, with the scalar form factor at the Cheng-Dashen point and the LECs  $c_3$  and  $c_4$ , which are less precise. As far as  $\sigma(2\mu^2)$  is concerned, we rely on the results [28]  $\sigma(2\mu^2) - \sigma(0) = 15.2 \pm 0.4$  MeV and  $\sigma(0) = 45 \pm 8$  MeV and adopt the central value  $\sigma(2\mu^2) = 60$  MeV. The values quoted for the LECs in the literature vary considerably, depending on the empirical input employed and the chiral order one is working at. A sample of values is given in Table I.

Our work is based on the  $\mathcal{O}(q^3)$  expansion of the intermediate  $\pi N$  amplitude and, for the sake of consistency, one must use LECs extracted at the same order. The kinematical conditions of the three-body interaction are such that the variable  $\nu$  is  $\mathcal{O}(q^2)$ , an order of magnitude smaller than the threshold value,  $\nu = \mu$ . This makes information encompassed in the subthreshold coefficients better suited to this problem and we use results from Appendix B to write

$$mc_3 = -mf_\pi^2 d_{01}^+ - \frac{g_A^4 m \mu}{16\pi f_\pi^2} - \frac{77g_A^2 m \mu}{768\pi f_\pi^2}, \quad (57)$$

$$mc_4 = \frac{f_\pi^2 b_{00}^-}{2} - \frac{1}{4} + \frac{g_A^2(1 + g_A^2)m\mu}{16\pi f_\pi^2}. \quad (58)$$

Adopting the values for the subthreshold coefficients given by Höhler [16], namely  $d_{01}^+ = 1.14 \pm 0.02 \mu^{-3}$  and  $b_{00}^- = 10.36 \pm 0.10 \mu^{-2}$ , one finds the figures shown in the last row of Table I. These, in turn, produce the strength coefficients displayed in Table II. For the sake of comparison, we also quote values employed in our earlier calculation [13] and in two TM' versions [31] of the Tucson-Melbourne potential [11].

Changes in these parameters represent theoretical progress achieved over more than two decades and it is worth investigating their origins in some detail. With this purpose in mind, we compare our present results with those of our previous  $\mathcal{O}(q^3)$  calculation [13]. At the chiral order at which one is working here, new qualitative effects begin to show up, associated with both loops and nonlocal interactions. They are represented by terms proportional to the coefficients  $C_3^+$ ,  $C_2^-$ , and  $C_3^-$  in Eqs. (45) and (46).

The  $\pi N$  coupling is now described by  $g_A^2 \mu^2 / f_\pi^2 = 3.66$  whereas, previously, the factor  $g^2 \mu^2 / m^2 = 3.97$  was used. From a conceptual point of view, the latter should be preferred, since  $g$  is indeed the proper coupling observable. In chiral

TABLE I. Some values of the LECs  $c_3$  and  $c_4$ ;  $m$  is the nucleon mass.

Reference	Chiral order	$\pi N$ input	$m c_3$	$m c_4$
[29]	3	amplitude at $\nu = 0$ , $t = 0$	$-5.00 \pm 1.43$	$3.62 \pm 0.04$
[29]	3	amplitude at $\nu = 0$ , $t = 2\mu^2/3$	$-5.01 \pm 1.01$	$3.62 \pm 0.04$
[30]	3	scattering amplitude	$-5.69 \pm 0.04$	$3.03 \pm 0.16$
[18]	4	subthreshold coefficients	-3.4	2.0
[18]	4	scattering lengths	-4.2	2.3
Tree	2	subthreshold coefficients	-3.6	2.0
This work	3	subthreshold coefficients	-4.9	3.3

TABLE II. Strength coefficients in MeV.

Reference	$C_1^+$	$C_2^+$	$C_3^+$	$C_1^-$	$C_2^-$	$C_3^-$
This work	0.794	-2.118	0.034	0.691	0.014	-0.067
Brazil [13]	0.92	-1.99	-	0.67	-	-
TM'(93) [31]	0.60	-2.05	-	0.58	-	-
TM'(99) [31]	0.91	-2.26	-	0.61	-	-

perturbation theory, the difference between both forms is ascribed to the parameter  $\Delta_{GT} = -2d_{18}\mu^2/g$ , which describes the Goldberger-Treiman discrepancy [18]. As this is a  $\mathcal{O}(q^2)$  effect, both forms of the coupling become equivalent in the present calculation. However, the empirical value of  $g$  is subject to larger uncertainties and the form based on  $g_A$  is more precise. Our present choice accounts for a decrease of 8% in all parameters.

The relations  $C_1^+ \leftrightarrow C_s$ ,  $C_2^+ \leftrightarrow C_p$ , and  $C_1^- \leftrightarrow -C'_p$  allow one to compare Eqs. (45) and (46) with Eq. (67) of Ref. [13]. One notes that the latter contains an unfortunate misprint in the sign of the term proportional to  $C'_p$ , as pointed out in Ref. [32]. In the earlier calculation, the coefficient  $C_s$  was based on a parameter [33]  $\alpha_\sigma = 1.05\mu^{-1}$ , which corresponds to  $\sigma(2\mu^2) = 64$  MeV. The results of Table II show that the values of  $C_2^+$  and  $C_1^-$  are rather close to those of  $C_p$  and  $-C'_p$ . This can be understood by rewriting Eqs. (52) and (54) in terms of the subthreshold coefficient  $d_{01}^+$  and  $b_{00}^-$  as follows:

$$C_2^+ = -\frac{g_A^2\mu^6}{32\pi^2 f_\pi^4 m} \left( m f_\pi^2 d_{01}^+ + \frac{g_A^2}{8} + \left[ \frac{29g_A^2 m \mu}{768\pi f_\pi^2} \right] \right), \quad (59)$$

$$C_1^- = \frac{g_A^2\mu^6}{128\pi^2 f_\pi^4 m} \left( f_\pi^2 b_{00}^- + \left[ \frac{g_A^2 m \mu}{16\pi f_\pi^2} \right] \right). \quad (60)$$

Numerically, this amounts to  $C_2^+ = -(1.845 + 0.110 + [0.163])$  MeV and  $C_1^- = (0.624 + [0.067])$  MeV. The second term in the former equation was overlooked in Ref. [13] and should have been considered there. The square brackets<sup>2</sup> correspond to next-to-leading order contributions and yield corrections of about 8% and 11% to the leading terms in  $C_2^+$  and  $C_1^-$ , respectively.<sup>3</sup> As the model used in Ref. [13] was explicitly designed to reproduce the subthreshold coefficients quoted by Höhler [16], it produces the very same contributions as the first terms in Eqs. (59) and (60).

## VI. NUMERICAL RESULTS FOR THREE-NUCLEON SYSTEMS

To test the effects of the TPE-3NP at  $\mathcal{O}(q^4)$ , in this section, we present some numerical results of Faddeev calculations for three-nucleon bound and scattering states. The calculations are

<sup>2</sup>These factors can be traced back to loop diagrams in Fig. 3 and are dynamically related to the term proportional to  $C_3^\pm$ , as we discuss in Appendix C.

<sup>3</sup>When comparing the new coefficients with those in the second row of Table II, one should also take into account the 8% effect from the Goldberger-Treiman discrepancy.

based on a configuration space approach, in which we solve the Faddeev integral equations [34–36],

$$\Phi_3 = \Xi_{12,3} + \frac{1}{E + i\epsilon - H_0 - V_{12}} \times [V_{12}(\Phi_1 + \Phi_2) + W_3(\Phi_1 + \Phi_2 + \Phi_3)]$$

(and cyclic permutations), (61)

where  $\Xi_{12,3}$ , which does not appear in the bound-state problem, is an initial state wave function for the scattering problem,  $H_0$  is a three-body kinetic operator in the center-of-mass frame,  $V_{12}$  is a nucleon-nucleon (2NP) potential between nucleons 1 and 2, and  $W_3$  is the 3NP displayed in Fig. 2. Partial wave states of a  $3N$  system, in which both  $NN$  and  $3N$  forces act, are restricted to those with total  $NN$  angular momenta  $j \leq 6$  for bound-state calculations, and  $j \leq 3$  for scattering-state calculations. The total  $3N$  angular momentum ( $J$ ) is truncated at  $J = 19/2$ , while 3NP is switched off for  $3N$  states with  $J > 9/2$  for scattering calculations. These truncation procedures are confirmed to give converged results for the purposes of the present work.

When just local terms are retained,  $\bar{t}_3$  in Eq. (43) can be cast in the conventional form [11–13]

$$\bar{t}_3 = -\frac{g_A^2}{4f_\pi^2} \frac{F(\mathbf{k}^2)}{\mathbf{k}^2 + \mu^2} \frac{F(\mathbf{k}'^2)}{\mathbf{k}'^2 + \mu^2} (\boldsymbol{\sigma}^{(1)} \cdot \mathbf{k})(\boldsymbol{\sigma}^{(2)} \cdot \mathbf{k}') \times [(\boldsymbol{\tau}^{(1)} \cdot \boldsymbol{\tau}^{(2)})\{a + b(\mathbf{k} \cdot \mathbf{k}')\} - (i\boldsymbol{\tau}^{(1)} \times \boldsymbol{\tau}^{(2)} \cdot \boldsymbol{\tau}^{(3)}) \times (i\boldsymbol{\sigma}^{(3)} \cdot \mathbf{k}' \times \mathbf{k})d], \quad (62)$$

where the coefficients  $a$ ,  $b$ , and  $d$  are related to our potential strength coefficients by

$$[C_1^+, C_2^+, C_1^-] = \frac{1}{(4\pi)^2} \left( \frac{g_A}{2f_\pi} \right)^2 [-a\mu^4, b\mu^6, -d\mu^6]. \quad (63)$$

The values of the coefficients  $a$ ,  $b$ , and  $d$  for the TPE-3NP at  $\mathcal{O}(q^4)$  are shown in Table III, as BR- $\mathcal{O}(q^4)$ . In this table, the values for the older version of the Brazil TPE-3NP, BR(83) [13], and the potential up to  $\mathcal{O}(q^3)$  given by Eqs. (41)–(42), BR- $\mathcal{O}(q^3)$ , are shown as well.

In Eq. (62), the function  $F(\mathbf{k}^2)$  represents a  $\pi NN$  form factor. We apply a dipole form factor with cutoff mass  $\Lambda$ ,  $\left( \frac{\Lambda^2 - \mu^2}{\Lambda^2 + \mathbf{k}^2} \right)^2$ , which modifies the profile functions  $U(x)$ ,  $U_1(x)$ , and  $U_2(x)$  in Eqs. (47)–(49) as

$$U(x) = \frac{e^{-x}}{x} - \frac{e^{-\bar{\Lambda}x}}{x} \left( 1 + \frac{\bar{\Lambda}^2 - 1}{2\bar{\Lambda}} x \right), \quad (64)$$

TABLE III. Coefficients  $a$ ,  $b$ , and  $d$  of the TPE-3NP.

3NP	$a \mu$	$b \mu^3$	$d \mu^3$
BR- $\mathcal{O}(q^4)$	-0.981	-2.617	-0.854
BR- $\mathcal{O}(q^3)$	-0.736	-3.483	-1.204
BR(83)	-1.05	-2.29	-0.768

$$U_1(x) = -\left(1 + \frac{1}{x}\right) \frac{e^{-x}}{x} + \bar{\Lambda}^2 \left(1 + \frac{1}{\bar{\Lambda}x}\right) \frac{e^{-\bar{\Lambda}x}}{\bar{\Lambda}x} + \left(\frac{\bar{\Lambda}^2 - 1}{2}\right) e^{-\bar{\Lambda}x}, \quad (65)$$

$$U_2(r) = \left(1 + \frac{3}{x} + \frac{3}{x^2}\right) \frac{e^{-x}}{x} - \bar{\Lambda}^3 \left(1 + \frac{3}{\bar{\Lambda}x} + \frac{3}{(\bar{\Lambda}x)^2}\right) \times \frac{e^{-\bar{\Lambda}x}}{\bar{\Lambda}x} - \frac{\bar{\Lambda}(\bar{\Lambda}^2 - 1)}{2} \left(1 + \frac{1}{\bar{\Lambda}x}\right) e^{-\bar{\Lambda}x}, \quad (66)$$

with  $\bar{\Lambda} = \Lambda/\mu$ .

We choose the Argonne  $V_{18}$  model (AV18) [9] for a realistic  $NN$  potential, by which the triton binding energy ( $B_3$ ) becomes 7.626 MeV, underbinding it by about 0.9 MeV compared to the empirical value, 8.482 MeV. As is well known, the introduction of the TPE-3NP remedies this deficiency. The amount of attractive contribution depends on the cutoff mass  $\Lambda$ , as shown in Fig. 5. The solid curve shows the dependence of  $B_3$  on  $\Lambda$  for the calculation with the BR- $\mathcal{O}(q^4)$  3NP in addition to the AV18 2NP [AV18 + BR- $\mathcal{O}(q^4)$ ]. In the figure, the empirical value and the AV18 result are displayed by the dashed and dotted horizontal lines, respectively. Owing to the strong attractive character of the 3NP,  $B_3$  is reproduced by choosing a rather small value of  $\Lambda$ , namely 660 MeV. In the same figure, the  $\Lambda$  dependence of  $B_3$  for AV18 + BR- $\mathcal{O}(q^3)$  is displayed by a dashed curve and that for the AV18 + BR(83) by a dotted curve. From these curves we see that AV18 + BR- $\mathcal{O}(q^3)$  reproduces  $B_3$  for  $\Lambda = 620$  MeV and AV18 + BR(83) for  $\Lambda = 680$  MeV. In other words, the BR- $\mathcal{O}(q^4)$  3NP is slightly more attractive than the BR(83) 3NP and a large attractive effect occurs when one moves from the TPE  $\mathcal{O}(q^4)$  3NP to the  $\mathcal{O}(q^3)$  3NP. This tendency is strongly correlated with the magnitude of the coefficient  $b$ , as shown in Table III. This can be understood as a dominant contribution to  $B_3$  from the component of the TPE-3NP associated with the coefficients  $b$ . This dominance is shown in Table IV, where we tabulate calculated  $B_3$  for the AV18 plus the BR- $\mathcal{O}(q^4)$  3NP and plus

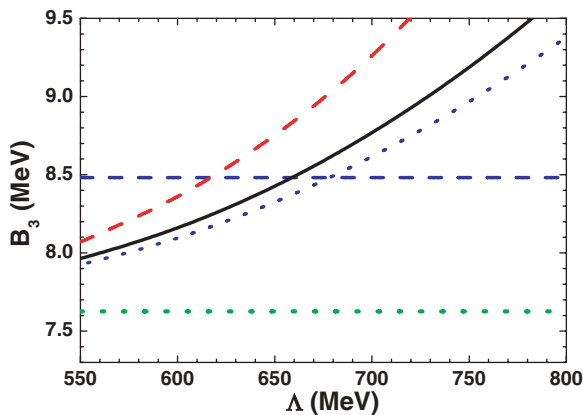


FIG. 5. (Color online) The triton binding energy  $B_3$  as functions of the cutoff mass  $\Lambda$  of the  $\pi NN$  dipole form factor. The solid curve denotes the result for AV18 + BR- $\mathcal{O}(q^4)$ , the dashed curve for AV18 + BR- $\mathcal{O}(q^3)$ , and the dotted curve for AV18 + BR(83). The horizontal lines denote the AV18 result (dotted line) and the empirical value (dashed line).

TABLE IV. Triton binding energy for the AV18 2NP plus the BR- $\mathcal{O}(q^4)$  3NP for each term of the BR- $\mathcal{O}(q^4)$  3NP with  $\Lambda = 660$  MeV.  $\Delta B_3$  means the difference of the calculated binding energy from that of the AV18 calculation.

	$B_3$ (MeV)	$\Delta B_3$ (MeV)
AV18 + BR- $\mathcal{O}(q^4)$	8.492	0.866
AV18 + BR- $\mathcal{O}(q^4)$ -a	7.673	0.047
AV18 + BR- $\mathcal{O}(q^4)$ -b	8.241	0.615
AV18 + BR- $\mathcal{O}(q^4)$ -d	7.787	0.161

each term of the BR- $\mathcal{O}(q^4)$  coming from the coefficients  $a$ ,  $b$ , and  $d$ .

In Fig. 6, we compare six calculated observables for proton-deuteron elastic scattering, namely differential cross sections  $\sigma(\theta)$ , vector analyzing powers of the proton  $A_y(\theta)$  and of the deuteron  $iT_{11}(\theta)$ , and tensor analyzing powers of the deuteron  $T_{20}(\theta)$ ,  $T_{21}(\theta)$ , and  $T_{22}(\theta)$ , at incident proton energy  $E_N^{\text{lab}} = 3.0$  MeV (or incident deuteron energy  $E_d^{\text{lab}} = 6.0$  MeV) with experimental data of Refs. [37,38]. In the figure, the solid curves designate the AV18 calculations and the dashed curves the AV18 + BR- $\mathcal{O}(q^4)$  calculations, which are almost indistinguishable from the AV18 + BR- $\mathcal{O}(q^3)$  and AV18 + BR(83) calculations, once the cutoff masses are chosen so that  $B_3$  is reproduced.

Recall that the TPE-3NF has a minor effect on the vector analyzing powers. This happens because the exchange of pions gives essentially scalar and tensor components of nuclear interaction in spin space, which are not so effective to the vector analyzing powers. However, as is noticed in Refs. [39,40], at  $E_N^{\text{lab}} = 3.0$  MeV, the TPE-3NP gives an incorrect contribution to the tensor analyzing power  $T_{21}(\theta)$  around  $\theta = 90^\circ$ .

In Fig. 7, we compare calculations of observables in neutron-deuteron elastic scattering at  $E_N^{\text{lab}} = 28.0$  MeV with experimental data of proton-deuteron scattering of Ref. [41]. At this energy, discrepancies between the calculations and the experimental data in the vector analyzing power  $iT_{11}(\theta)$  appear at  $\theta \sim 100^\circ$ , where  $iT_{11}(\theta)$  has a minimum, and at  $\theta \sim 140^\circ$ , where  $iT_{11}(\theta)$  has a maximum, which are not compensated by the introduction of the TPE-3NP. However, whereas the AV18 calculation almost reproduces the experimental data of  $T_{21}(\theta)$  at  $\theta \sim 90^\circ$ , the introduction of the TPE-3NP gives an incorrect effect, as in the  $E_N^{\text{lab}} = 3$  MeV case.

These results set the stage for the introduction of terms associated with the coefficients  $C_3^+$ ,  $C_2^-$ , and  $C_3^-$ , Eqs. (44)–(45), which are new features of the  $\mathcal{O}(q^4)$  expansion of the TPE-3NP. Terms proportional to  $C_3^\pm$ , which include the rather complicated function  $I(\mathbf{r}_{31}, \mathbf{r}_{23})$  given in Appendix C, arise from a loop integral, Eq. (33). The term with  $C_2^-$  corresponds to a nonlocal potential and includes the gradient operator  $\nabla_{ij}^{wf}$ , which acts on the wave function and arises from the kinematical variable  $\nu$ . Both kinds of contributions are not expressed in the conventional local form shown in Eq. (62), which involves only the coefficients  $C_1^+$ ,  $C_2^+$ , and  $C_1^-$ , and the full evaluation of their effects would require an extensive rebuilding of large numerical codes. However, the coefficients

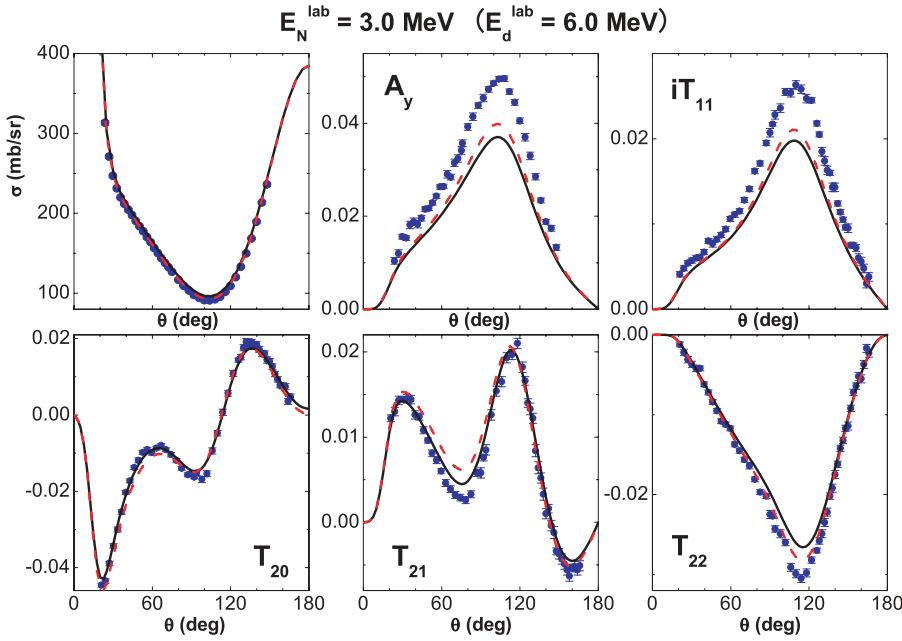


FIG. 6. (Color online) Proton-deuteron elastic scattering observables at  $E_N^{\text{lab}} = 3.0$  MeV. Solid curves are calculations for the AV18 potential and dashed curves for the AV18 + BR- $\mathcal{O}(q^4)$ . Experimental data are taken from Refs. [37,38].

of the new terms are small, and in this exploratory paper we estimate their influence over observables as follows.

The function  $I(\mathbf{r}_{31}, \mathbf{r}_{23})$  is approximated by Eq. (C11), which amounts to replacing  $\Pi_t(t)$  by a factor  $-\pi$ . Further, the kinematical factors in front of  $\Pi_t(t)$  in Eqs. (34) and (38), namely  $1 - 2t/\mu^2$  and  $1 - t/4\mu^2$ , are approximately evaluated by putting  $t \approx 2\mu^2$ , which yields  $-3$  and  $1/2$ , respectively. By this procedure, the coefficients  $C_3^+$  and  $C_3^-$  are absorbed into  $C_2^+$  and  $C_1^-$ , or in  $b$  and  $d$ , respectively, and one has

$$\Delta C_2^+ = -3C_3^+, \quad \Delta C_1^- = C_3^-/2. \quad (67)$$

Numerically, this corresponds to  $\Delta C_2^+ = -0.102$  MeV  $\sim \frac{1}{20}C_2^+$  and  $\Delta C_1^- = -0.034$  MeV  $\sim -\frac{1}{20}C_1^-$ , or  $\Delta b = -0.125(\mu^{-3})$  and  $\Delta d = 0.042(\mu^{-3})$ . The net change produced in the triton binding energy is  $+0.026$  MeV ( $+0.037$  MeV from  $\Delta C_2^+$  and  $-0.011$  MeV from  $\Delta C_1^-$ ), just about 1/30 of the total increase in  $B_3$  owing to the local terms of the BR- $\mathcal{O}(q^4)$  TPE-3NP.

The nonlocal term proportional to  $C_2^-$  is more involved and we restrict ourselves to a rough assessment of its role. We replace the variable  $\nu$  by a constant  $\langle \nu \rangle$  and assume, for example, that  $\langle \nu \rangle = \frac{\mu^2}{4m}$ . This changes the  $C_2^-$  term in Eq. (46)

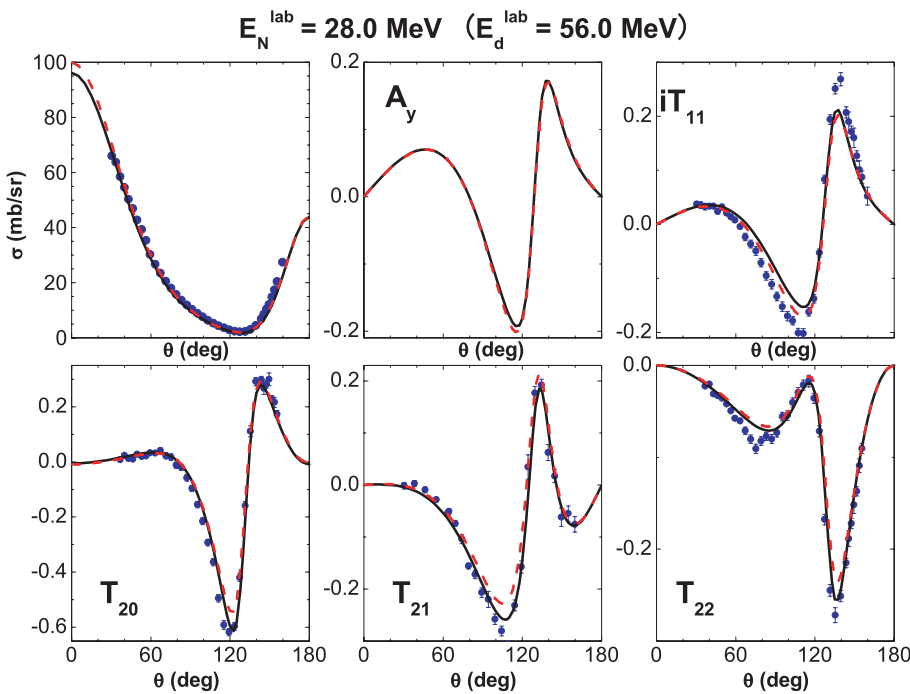


FIG. 7. (Color online) Nucleon-deuteron elastic scattering observables at  $E_N^{\text{lab}} = 28.0$  MeV. Curves are calculations for neutron-deuteron scattering. Solid curves denote calculations for the AV18 potential and dashed curves for the AV18 + BR- $\mathcal{O}(q^4)$ . Experimental data are those for proton-deuteron scattering taken from Ref. [41].

into the very simple form

$$V_3^-(\mathbf{r}, \boldsymbol{\rho}) = C_1^-(\dots) + i\tilde{C}_2^-\boldsymbol{\sigma}^{(1)} \cdot \hat{\mathbf{x}}_{31}\boldsymbol{\sigma}^{(2)} \cdot \hat{\mathbf{x}}_{23}U_1(x_{31})U_1(x_{23}) + C_3^-(\dots), \quad (68)$$

with

$$\begin{aligned} \tilde{C}_2^- &= -\frac{g_A^2}{4f_\pi^2} \frac{1-g_A^2}{2f_\pi^2} \langle v \rangle \frac{\mu^4}{(4\pi)^2} \\ &= -\frac{g_A^2(1-g_A^2)\mu^6}{512\pi^2 f_\pi^4 m} = 0.021 \text{ MeV}. \end{aligned} \quad (69)$$

Except for the isospin factor, this term is similar to that with  $C_1^+$  (or  $a$ ), which adds about 0.05 MeV to the triton binding energy. Since the potential strength  $\tilde{C}_2^-$  is about 3% of  $C_1^+$ , its contribution to the binding energy may be estimated to be a tiny 0.001 MeV.

## VII. CONCLUSIONS

In the framework of chiral perturbation theory, three-nucleon forces begin at  $\mathcal{O}(q^3)$ , with a simple long-range component from the exchanges of two pions. At  $\mathcal{O}(q^4)$ , in contrast, a large number of different processes intervene and a full description becomes rather complex. For this reason, here we concentrate on a subset of  $\mathcal{O}(q^4)$  interactions, namely that which still involves the exchanges of just two pions. This part of the 3NP is closely related to the  $\pi N$  amplitude, and the expansion of the former up to  $\mathcal{O}(q^4)$  depends on the latter at  $\mathcal{O}(q^3)$ .

Our expressions for the potential are given in Eqs. (44)–(56) and the new chiral layer of the TPE-3NP considered in this work gives rise to both numerical corrections to strength coefficients of already existing terms ( $C_1^+$ ,  $C_2^+$ ,  $C_1^-$ ) and new structures in the profile functions. Changes in numerical coefficients lay in the neighborhood of 10% and can be read in Tables II and III. New structures, however, arise either from loop functions representing form factors or the nonlocal terms associated with gradients acting on the wave function. They correspond to the terms proportional to the parameters  $C_3^+$ ,  $C_2^-$ , and  $C_3^-$ , which are small and compatible with perturbative effects.

To insert our results into a broader picture, in Table V we show the orders at which the various effects begin to appear, including the drift potential derived recently [42].

The influence of the new TPE-3NP over three-body observables has been assessed in both static and scattering environments, by adopting the Argonne  $V_{18}$  potential for the two-body interaction. To reproduce the empirical triton binding energy, the  $\mathcal{O}(q^4)$  potential requires a cutoff mass of

660 MeV. Comparing this with the value of 680 MeV for the 1983 Brazil TPE-3NP, one learns that the later version is more attractive.

In the study of proton-deuteron elastic scattering, we have calculated cross sections  $\sigma(\theta)$ , vector analyzing powers  $A_y(\theta)$  of the proton and  $iT_{11}(\theta)$  of the deuteron, and tensor analyzing powers  $T_{20}(\theta)$ ,  $T_{21}(\theta)$ , and  $T_{22}(\theta)$  of the deuteron, at energies of 3 and 28 MeV. The results are displayed in Figs. 6 and 7, where it is possible to see that there is little sensitivity to the changes induced in the strength parameters when one goes from  $\mathcal{O}(q^3)$  to  $\mathcal{O}(q^4)$ . Old problems, such as the  $A_y(\theta)$  puzzle, remain unsolved.

The present version of the TPE-3NP contains new structures, associated with loop integrals and nonlocal operators. Their influence over observables has been estimated and found to be at least one order of magnitude smaller than other three-body effects. A more detailed study of this part of the force is being carried out.

## APPENDIX A: KINEMATICS

The coordinate describing the position of nucleon  $i$  is  $\mathbf{r}_i$  and one uses the combinations

$$\begin{aligned} \mathbf{R} &= (\mathbf{r}_1 + \mathbf{r}_2 + \mathbf{r}_3)/3, & \mathbf{r} &= \mathbf{r}_2 - \mathbf{r}_1, \\ \boldsymbol{\rho} &= (2\mathbf{r}_3 - \mathbf{r}_1 - \mathbf{r}_2)/\sqrt{3}, \end{aligned} \quad (A1)$$

which yield

$$\begin{aligned} \mathbf{r}_1 &= \mathbf{R} - \frac{\mathbf{r}}{2} - \frac{\boldsymbol{\rho}}{2\sqrt{3}}, & \mathbf{r}_2 &= \mathbf{R} + \frac{\mathbf{r}}{2} - \frac{\boldsymbol{\rho}}{2\sqrt{3}}, \\ \mathbf{r}_3 &= \mathbf{R} + \frac{\boldsymbol{\rho}}{\sqrt{3}}. \end{aligned} \quad (A2)$$

The momentum of nucleon  $i$  is  $\mathbf{p}_i$  and one defines

$$\begin{aligned} \mathbf{P} &= \mathbf{p}_1 + \mathbf{p}_2 + \mathbf{p}_3, & \mathbf{p}_r &= (\mathbf{p}_2 - \mathbf{p}_1)/2, \\ \mathbf{p}_\rho &= (2\mathbf{p}_3 - \mathbf{p}_1 - \mathbf{p}_2)/2\sqrt{3}. \end{aligned} \quad (A3)$$

Initial momenta  $\mathbf{p}$  and final momenta  $\mathbf{p}'$  are used in the combinations

$$\mathbf{Q} = (\mathbf{P}' + \mathbf{P})/2, \quad \mathbf{q} = (\mathbf{P}' - \mathbf{P}), \quad (A4)$$

$$\mathbf{Q}_r = (\mathbf{p}'_r + \mathbf{p}_r)/2, \quad \mathbf{q}_r = (\mathbf{p}'_r - \mathbf{p}_r), \quad (A5)$$

$$\mathbf{Q}_\rho = (\mathbf{p}'_\rho + \mathbf{p}_\rho)/2, \quad \mathbf{q}_\rho = (\mathbf{p}'_\rho - \mathbf{p}_\rho). \quad (A6)$$

In the center of mass, one has  $\mathbf{P} = 0$  and the three-momenta are given by

$$\begin{aligned} \mathbf{p}_1 &= -(\mathbf{Q}_r - \mathbf{q}_r/2) - (\mathbf{Q}_\rho - \mathbf{q}_\rho/2)/\sqrt{3}, \\ \mathbf{p}'_1 &= -(\mathbf{Q}_r + \mathbf{q}_r/2) - (\mathbf{Q}_\rho + \mathbf{q}_\rho/2)/\sqrt{3}, \end{aligned} \quad (A7)$$

TABLE V. Chiral picture for two- and three-body forces.

Beginning	Two-body	Two-body	Three-body
$\mathcal{O}(q^0)$	OPEP: $V_T^-, V_{SS}^-$		
$\mathcal{O}(q^2)$	OPEP: $V_D^-$	TPEP: $V_C^-; V_T^+, V_{SS}^+$	
$\mathcal{O}(q^3)$		TPEP: $V_{LS}^-, V_T^-, V_{SS}^-; V_C^+, V_{LS}^+$	TPEP: $C_1^-; C_1^+, C_2^+$
$\mathcal{O}(q^4)$		TPEP: $V_D^-; V_Q^+, V_D^+$	TPEP: $C_2^-; C_3^-, C_3^+$

$$\begin{aligned} p_2 &= (\mathbf{Q}_r - \mathbf{q}_r/2) - (\mathbf{Q}_\rho - \mathbf{q}_\rho/2)/\sqrt{3}, \\ p'_2 &= (\mathbf{Q}_r + \mathbf{q}_r/2) - (\mathbf{Q}_\rho + \mathbf{q}_\rho/2)/\sqrt{3}, \end{aligned} \quad (\text{A8})$$

$$\begin{aligned} p_3 &= 2(\mathbf{Q}_\rho - \mathbf{q}_\rho/2)/\sqrt{3}, \\ p'_3 &= 2(\mathbf{Q}_\rho + \mathbf{q}_\rho/2)/\sqrt{3}. \end{aligned} \quad (\text{A9})$$

Energy conservation for on-shell particles yield the nonrelativistic constraint

$$\mathbf{Q}_r \cdot \mathbf{q}_r + \mathbf{Q}_\rho \cdot \mathbf{q}_\rho = 0. \quad (\text{A10})$$

The momenta of the exchanged pions are written as

$$k = p_1 - p'_1, \quad k' = p'_2 - p_2, \quad (\text{A11})$$

$$k^0 = -(\mathbf{q}_r + \mathbf{q}_\rho/\sqrt{3}) \cdot (\mathbf{Q}_r + \mathbf{Q}_\rho/\sqrt{3})/m, \quad (\text{A12})$$

$$\mathbf{k} = \mathbf{q}_r + \mathbf{q}_\rho/\sqrt{3},$$

$$k'^0 = (\mathbf{q}_r - \mathbf{q}_\rho/\sqrt{3}) \cdot (\mathbf{Q}_r - \mathbf{Q}_\rho/\sqrt{3})/m, \quad (\text{A13})$$

$$\mathbf{k}' = \mathbf{q}_r - \mathbf{q}_\rho/\sqrt{3},$$

and the Mandelstam variables for nucleon 3 read

$$\begin{aligned} s &= (p_3 + k)^2 = m^2 - (\mathbf{q}_r + \mathbf{q}_\rho/\sqrt{3}) \\ &\cdot (\mathbf{q}_r + 2\mathbf{Q}_r - \mathbf{q}_\rho/\sqrt{3} + 2\sqrt{3}\mathbf{Q}_\rho) + \mathcal{O}(q^4), \end{aligned} \quad (\text{A14})$$

$$\begin{aligned} u &= (p_3 - k')^2 = m^2 - (\mathbf{q}_r - \mathbf{q}_\rho/\sqrt{3}) \\ &\cdot (\mathbf{q}_r + 2\mathbf{Q}_r + \mathbf{q}_\rho/\sqrt{3} - 2\sqrt{3}\mathbf{Q}_\rho) + \mathcal{O}(q^4), \end{aligned} \quad (\text{A15})$$

$$v = (s - u)/4m = -2\mathbf{q}_r \cdot \mathbf{Q}_\rho/\sqrt{3} + \mathcal{O}(q^4). \quad (\text{A16})$$

In the evaluation of the intermediate  $\pi N$  amplitude, one needs

$$[\bar{u}(\mathbf{p}')u(\mathbf{p})]^{(3)} \simeq 2m + \mathcal{O}(q^2), \quad (\text{A17})$$

$$\begin{aligned} &\left[ \frac{i}{2m} \bar{u}(\mathbf{p}') \sigma_{\mu\nu} (p' - p)^\mu K^\nu u(\mathbf{p}) \right]^{(3)} \\ &\simeq 2i\boldsymbol{\sigma}^{(3)} \cdot \mathbf{q}_\rho \times \mathbf{q}_r/\sqrt{3} + \mathcal{O}(q^4). \end{aligned} \quad (\text{A18})$$

The  $\pi N$  vertex for nucleon 1 is associated with

$$[\bar{u}(\mathbf{p}')\gamma_3 u(\mathbf{p})]^{(1)} \simeq \boldsymbol{\sigma}^{(1)} \cdot (\mathbf{q}_r + \mathbf{q}_\rho/\sqrt{3}) + \mathcal{O}(q^3), \quad (\text{A19})$$

and results for nucleon 2 are obtained by making  $\mathbf{q}_r \rightarrow -\mathbf{q}_r$ .

## APPENDIX B: SUBTHRESHOLD COEFFICIENTS

The polynomial parts of the amplitudes  $T_R^\pm$ , Eqs. (16)–(19), are determined by the subthreshold coefficients of Ref. [18]. The terms relevant to the  $\mathcal{O}(q^3)$  expansion are written as [6]

$$d_{00}^+ = -\frac{2(2c_1 - c_3)\mu^2}{f_\pi^2} + \frac{8g_A^4\mu^3}{64\pi f_\pi^4} + \left[ \frac{3g_A^2\mu^3}{64\pi f_\pi^4} \right]_{mr}, \quad (\text{B1})$$

$$d_{01}^+ = -\frac{c_3}{f_\pi^2} - \frac{48g_A^4\mu}{768\pi f_\pi^4} - \left[ \frac{77g_A^2\mu}{768\pi f_\pi^4} \right]_{mr}, \quad (\text{B2})$$

$$d_{02}^+ = \left[ \frac{193g_A^2}{15360\pi f_\pi^4\mu} \right]_{mr}, \quad (\text{B3})$$

$$d_{00}^- = \left[ \frac{1}{2f_\pi^2} \right]_{WT} + \mathcal{O}(q^2), \quad (\text{B4})$$

$$b_{00}^- = \left[ \frac{1}{2f_\pi^2} \right]_{WT} + \frac{2c_4 m}{f_\pi^2} - \frac{g_A^4 m \mu}{8\pi f_\pi^4} - \left[ \frac{g_A^2 m \mu}{8\pi f_\pi^4} \right]_{mr}, \quad (\text{B5})$$

$$b_{01}^- = \left[ \frac{g_A^2 m}{96\pi f_\pi^4 \mu} \right]_{mr}, \quad (\text{B6})$$

where the parameters  $c_i$  are the usual coupling constants of the chiral Lagrangians of order 2 [43]. Terms within square brackets labeled ( $mr$ ) in these results are due to the medium-range diagrams shown in Fig. 3 and have been included explicitly into the functions  $D_{mr}^\pm$  and  $B_{mr}^\pm$ . Terms bearing the ( $WT$ ) label were also explicitly considered in Eqs. (15)–(19). The subthreshold coefficients are determined from  $\pi N$  scattering data and a set of experimental values is given in Ref. [16].

## APPENDIX C: FUNCTIONS $I^n$

The functions  $I^n$ , describing loop contributions, are given by

$$\begin{aligned} I^n(\mathbf{r}_{31}, \mathbf{r}_{23}) &= -\frac{16\pi}{\mu^2} \int \frac{d\mathbf{k}}{(2\pi)^3} \frac{d\mathbf{k}'}{(2\pi)^3} e^{i(\mathbf{k}\cdot\mathbf{r}_{31} + \mathbf{k}'\cdot\mathbf{r}_{23})} \left[ \frac{t}{\mu^2} \right]^n \\ &\times \frac{1}{k^2 + \mu^2} \frac{1}{k'^2 + \mu^2} \Pi_1(t). \end{aligned} \quad (\text{C1})$$

Using the definition Eq. (33) and the Jacobi variables Eq. (A1), one writes

$$I^n(\mathbf{r}_{31}, \mathbf{r}_{23}) = \left[ \frac{4\nabla_\rho^2}{3\mu^2} \right]^n I(\mathbf{r}_{31}, \mathbf{r}_{23}), \quad (\text{C2})$$

$$I(\mathbf{r}_{31}, \mathbf{r}_{23}) = 128\pi \int_0^1 da \tan^{-1} \left[ \frac{ma\sqrt{1-a^2}}{\mu(1-a^2/2)} \right] L(a; \mathbf{r}, \boldsymbol{\rho}), \quad (\text{C3})$$

$$\begin{aligned} L(a; \mathbf{r}, \boldsymbol{\rho}) &= \int \frac{d\mathbf{q}}{(2\pi)^3} \frac{d\mathbf{Q}}{(2\pi)^3} \frac{e^{i(\mathbf{Q}\cdot\mathbf{r} - \sqrt{3}\mathbf{q}\cdot\boldsymbol{\rho}/2)}}{a^2 q^2 + 4\mu^2} \\ &\times \frac{1}{[(\mathbf{Q} - \mathbf{q})^2 + \mu^2]} \frac{1}{[(\mathbf{Q} + \mathbf{q})^2 + \mu^2]}. \end{aligned} \quad (\text{C4})$$

The numerical evaluation of the function  $L$  can be simplified by using alternative representations.

Form 1: One uses the Feynman procedure for manipulating denominators, which yields

$$\begin{aligned} L(a; \mathbf{r}, \boldsymbol{\rho}) &= \int_0^1 db \int \frac{d\mathbf{q}}{(2\pi)^3} \frac{d\mathbf{Q}}{(2\pi)^3} \frac{e^{i(\mathbf{Q}\cdot\mathbf{r} - \sqrt{3}\mathbf{q}\cdot\boldsymbol{\rho}/2)}}{a^2 q^2 + 4\mu^2} \\ &\times \frac{1}{[(\mathbf{Q}^2 + \mathbf{q}^2/4 + \mu^2) - (1-2b)\mathbf{q}\cdot\mathbf{Q}]^2} \\ &= \frac{1}{8\pi} \int_0^1 db \int \frac{d\mathbf{q}}{(2\pi)^3} \frac{e^{i[(1-2b)\mathbf{r} - \sqrt{3}\boldsymbol{\rho}]\cdot\mathbf{q}/2}}{a^2 q^2 + 4\mu^2} \frac{e^{-\Theta r}}{\Theta}, \\ &\Theta = \sqrt{\mu^2 + b(1-b)\mathbf{q}^2}. \end{aligned} \quad (\text{C5})$$

Performing the angular integration over  $\mathbf{q}$ , one has

$$L(a; \mathbf{r}, \boldsymbol{\rho}) = \frac{1}{16\pi^3} \int_0^1 db \int d\mathbf{q} q \frac{e^{-\Theta r}}{\Theta(a^2 q^2 + 4\mu^2)} \times \frac{\sin q[(1-2b)\mathbf{r} - \sqrt{3}\boldsymbol{\rho}]/2}{[(1-2b)\mathbf{r} - \sqrt{3}\boldsymbol{\rho}]/2}. \quad (\text{C6})$$

Form 2: The Fourier transform

$$\frac{1}{\mathbf{k}^2 + \mu^2} = \int d\mathbf{x} e^{-i\mathbf{k}\cdot\mathbf{x}} \frac{e^{-\mu x}}{4\pi x} \quad (\text{C7})$$

allows one to write

$$L(a; \mathbf{r}, \boldsymbol{\rho}) = \frac{1}{64\pi^3} \frac{1}{a^2} \int dz \frac{e^{-\mu|r_{31}+z|} e^{-\mu|r_{23}-z|} e^{-2\mu z/a}}{|r_{31}+z| |r_{23}-z| z}. \quad (\text{C8})$$

These results may be further simplified by means of approximations.

Heavy-baryon approximation: In the limit  $m \rightarrow \infty$ , corresponding to the heavy-baryon case, one uses  $F(a) \rightarrow 4\pi/a^2$  in Eq. (33) and Eqs. (C5) and (C7) yield, respectively,

$$I(\mathbf{r}_{31}, \mathbf{r}_{23}) \simeq \frac{2}{\pi} \int_0^1 db \int_0^\infty dq \left[ \tan^{-1} \frac{q}{2\mu} \right] \frac{e^{-\Theta r}}{\mu\Theta} \times \frac{\sin q[(1-2b)\mathbf{r} - \sqrt{3}\boldsymbol{\rho}]/2}{[(1-2b)\mathbf{r} - \sqrt{3}\boldsymbol{\rho}]/2}, \quad (\text{C9})$$

$$I(\mathbf{r}_{31}, \mathbf{r}_{23}) \simeq \frac{1}{\pi} \int dz \frac{e^{-\mu|r_{31}+z|} e^{-\mu|r_{23}-z|} e^{-2\mu z}}{|r_{31}+z| |r_{23}-z| 2\mu z^2}. \quad (\text{C10})$$

Multipole approximation: The integrand in Eq. (C10) is peaked around  $z = 0$  and a multipole expansion of the Yukawa functions produces

$$I(\mathbf{r}_{31}, \mathbf{r}_{23}) \simeq U(x_{31})U(x_{23}) + \dots \quad (\text{C11})$$

The same result can also be obtained by using the expansion  $\Pi_i(t) \sim -\pi[1 + t/12\mu^2 + t^2/80\mu^4 + \dots]$ , valid for low  $t$ , directly into Eq. (C1).

#### APPENDIX D: NONLOCAL TERM

In configuration space, the variable  $\mathbf{Q}_\rho$  corresponds to a nonlocal operator, represented by a gradient acting on the wave function. To make the dependence of  $\bar{t}_3$  on  $\mathbf{Q}_\rho$  explicit, one writes

$$\bar{t}_3 = [\mathbf{Q}_\rho]_i X_i(\mathbf{q}_r, \mathbf{q}_\rho), \quad (\text{D1})$$

where  $X$  is a generic three-vector, and evaluates the matrix element

$$\begin{aligned} \langle \psi | W | \psi \rangle &= - \left[ \frac{1}{(2\pi)} \right]^{12} \int d\mathbf{r}' d\boldsymbol{\rho}' d\mathbf{r} d\boldsymbol{\rho} \psi^*(\mathbf{r}', \boldsymbol{\rho}') \psi(\mathbf{r}, \boldsymbol{\rho}) \\ &\times \int d\mathbf{Q}_r d\mathbf{Q}_\rho d\mathbf{q}_r d\mathbf{q}_\rho \\ &\times e^{i[\mathbf{Q}_r \cdot (\mathbf{r}' - \mathbf{r}) + \mathbf{Q}_\rho \cdot (\boldsymbol{\rho}' - \boldsymbol{\rho}) + \mathbf{q}_r \cdot (\mathbf{r}' + \mathbf{r})/2 + \mathbf{q}_\rho \cdot (\boldsymbol{\rho}' + \boldsymbol{\rho})/2]} \\ &\times \bar{t}_3(\mathbf{Q}_r, \mathbf{Q}_\rho, \mathbf{q}_r, \mathbf{q}_\rho) \\ &= - \left[ \frac{1}{(2\pi)} \right]^6 \int d\mathbf{r} d\boldsymbol{\rho} \left\{ \left[ \frac{i}{2} \nabla_\rho \psi^*(\mathbf{r}, \boldsymbol{\rho}) \right]_i \right. \\ &\times \psi(\mathbf{r}, \boldsymbol{\rho}) + \psi^*(\mathbf{r}, \boldsymbol{\rho}) \left. \left[ -\frac{i}{2} \nabla_\rho \psi(\mathbf{r}, \boldsymbol{\rho}) \right]_i \right\} \\ &\times \int d\mathbf{q}_r d\mathbf{q}_\rho e^{i[\mathbf{q}_r \cdot \mathbf{r} + \mathbf{q}_\rho \cdot \boldsymbol{\rho}]} X_i(\mathbf{q}_r, \mathbf{q}_\rho). \quad (\text{D2}) \end{aligned}$$

This yields the potential

$$V_3(\mathbf{r}, \boldsymbol{\rho}) = - \frac{[2/\sqrt{3}]^3}{(2\pi)^6} \left[ -\frac{i}{2} \overset{\leftrightarrow}{\nabla}_\rho \right]_i \int d\mathbf{q}_r d\mathbf{q}_\rho e^{i[\mathbf{q}_r \cdot \mathbf{r} + \mathbf{q}_\rho \cdot \boldsymbol{\rho}]} \times X_i(\mathbf{q}_r, \mathbf{q}_\rho), \quad (\text{D3})$$

where the operator  $\overset{\leftrightarrow}{\nabla} = \overset{\leftarrow}{\nabla} - \overset{\rightarrow}{\nabla}$  acts *only* on the wave function. An alternative form can be obtained by integrating Eq. (D2) by parts, and one finds

$$\begin{aligned} V_3(\mathbf{r}, \boldsymbol{\rho}) &= - \frac{[2/\sqrt{3}]^3}{(2\pi)^6} \left\{ \left[ \int d\mathbf{q}_r d\mathbf{q}_\rho e^{i[\mathbf{q}_r \cdot \mathbf{r} + \mathbf{q}_\rho \cdot \boldsymbol{\rho}]} X(\mathbf{q}_r, \mathbf{q}_\rho) \right] \right. \\ &\cdot \left[ -i \nabla_\rho^{wf} \right] - \left. \left[ \frac{i}{2} \nabla_\rho \cdot \int d\mathbf{q}_r d\mathbf{q}_\rho e^{i[\mathbf{q}_r \cdot \mathbf{r} + \mathbf{q}_\rho \cdot \boldsymbol{\rho}]} \right] \right. \\ &\times \left. X(\mathbf{q}_r, \mathbf{q}_\rho) \right\}. \quad (\text{D4}) \end{aligned}$$

In the case of the three-body force, the only nonlocal contribution is associated with the subamplitude  $D^-$ , Eq. (37), which yields

$$\begin{aligned} X_i &= -i \boldsymbol{\tau}^{(1)} \times \boldsymbol{\tau}^{(2)} \cdot \boldsymbol{\tau}^{(3)} \frac{1}{\mathbf{k}^2 + \mu^2} \frac{1}{\mathbf{k}'^2 + \mu^2} \boldsymbol{\sigma}^{(1)} \cdot \mathbf{k} \boldsymbol{\sigma}^{(2)} \\ &\cdot \mathbf{k}' \left[ \frac{g_A^2 (g_A^2 - 1)}{\sqrt{38} f_\pi^4 m} \right] (\mathbf{k}' + \mathbf{k})_i. \quad (\text{D5}) \end{aligned}$$

The action of  $\nabla_\rho$  on the second term of Eq. (D4) gives rise to an integrand proportional to  $(\mathbf{k}'^2 - \mathbf{k}^2)$ , which has short range and does not contribute to the TPE-3NP. Therefore it is neglected.

- [1] M. Taketani, S. Nakamura, and T. Sasaki, Prog. Theor. Phys. **6**, 581 (1951).  
 [2] S. Weinberg, Phys. Lett. **B251**, 288 (1990); Nucl. Phys. **B363**, 3 (1991).  
 [3] S. Weinberg, Phys. Lett. **B295**, 114 (1992).  
 [4] C. Ordóñez and U. van Kolck, Phys. Lett. **B291**, 459 (1992);

- C. Ordóñez, L. Ray, and U. van Kolck, Phys. Rev. Lett. **72**, 1982 (1994); Phys. Rev. C **53**, 2086 (1996).  
 [5] N. Kaiser, R. Brockman, and W. Weise, Nucl. Phys. **A625**, 758 (1997); N. Kaiser, Phys. Rev. C **64**, 057001 (2001); Phys. Rev. C **65**, 017001 (2001); E. Epelbaum, W. Glöckle, and U-G. Meissner, Nucl. Phys. **A637**, 107 (1998); **A671**, 295 (2000);

- D. R. Entem and R. Machleidt, Phys. Rev. C **66**, 014002 (2002).
- [6] R. Higa and M. R. Robilotta, Phys. Rev. C **68**, 024004 (2003).
- [7] R. Higa, M. R. Robilotta, and C. A. da Rocha, Phys. Rev. C **69**, 034009 (2004).
- [8] J. C. Pupin and M. R. Robilotta, Phys. Rev. C **60**, 014003 (1999); N. Kaiser, *ibid.* **63**, 044010 (2001).
- [9] R. B. Wiringa, V. G. J. Stoks, and R. Schiavilla, Phys. Rev. C **51**, 38 (1995).
- [10] J. Fujita and H. Miyazawa, Prog. Theor. Phys. **17**, 360 (1957).
- [11] S. A. Coon, M. D. Scadron, P. C. McNamee, B. R. Barrett, D. W. E. Blatt, and B. H. J. McKellar, Nucl. Phys. **A317**, 242 (1979).
- [12] S. A. Coon and W. Glöckle, Phys. Rev. C **23**, 1790 (1981).
- [13] H. T. Coelho, T. K. Das, and M. R. Robilotta, Phys. Rev. C **28**, 1812 (1983).
- [14] J. L. Friar, Phys. Rev. C **60**, 034002 (1999).
- [15] S.-N. Yang, Phys. Rev. C **10**, 2067 (1974).
- [16] G. Höhler, *Landölt-Bornstein Numerical Data and Functional Relationships in Science and Technology*, Group I, Vol 9b, Part 2, edited by H. Schopper (Springer, New York, 1983); G. Höhler, H. P. Jacob, and R. Strauss, Nucl. Phys. **B39**, 273 (1972).
- [17] T. Becher and H. Leutwyler, Eur. Phys. J. C **9**, 643 (1999).
- [18] T. Becher and H. Leutwyler, J. High Energy Phys. **06** (2001) 017.
- [19] J. C. Ward, Phys. Rev. **78**, 1824 (1950); Y. Takahashi, Nuovo Cimento **6**, 371 (1957); L. S. Brown, W. J. Pardee, and R. Peccei, Phys. Rev. D **4**, 2801 (1971).
- [20] M. Mojžiš and J. Kambor, Phys. Lett. **B476**, 344 (2000).
- [21] J. Gasser, M. E. Sainio, and A. Švarc, Nucl. Phys. **B307**, 779 (1988).
- [22] G. Höhler, H. P. Jacob, and R. Strauss, Nucl. Phys. **B39**, 273 (1972).
- [23] S. Weinberg, Phys. Rev. Lett. **17**, 616 (1966).
- [24] Y. Tomozawa, Nuovo Cimento A **46**, 707 (1966).
- [25] M. R. Robilotta, Phys. Rev. C **63**, 044004 (2001).
- [26] I. P. Cavalcante, M. R. Robilotta, J. Sá Borges, D. de O. Santos, and G. R. S. Zarnauskas, Phys. Rev. C **72**, 065207 (2005).
- [27] J. L. Friar, D. Huber, and U. van Kolck, Phys. Rev. C **59**, 53 (1999); U. van Kolck, Ph. D. thesis, University of Texas, 1993; C. Ordóñez and U. van Kolck, Phys. Lett. **B291**, 459 (1992); U. van Kolck, Phys. Rev. C **49**, 2932 (1994).
- [28] J. Gasser, H. Leutwyler, and M. E. Sainio, Phys. Lett. **B253**, 252 (1991); **B253**, 260 (1991).
- [29] P. Büttiker and U.-G. Meissner, Nucl. Phys. **A668**, 97 (2000).
- [30] N. Fettes and U.-G. Meissner, Nucl. Phys. **A693**, 693 (2001).
- [31] S. A. Coon and H. K. Han, Few-Body Syst. **30**, 131 (2001).
- [32] M. R. Robilotta and H. T. Coelho, Nucl. Phys. **A460**, 645 (1986).
- [33] M. G. Olsson and E. T. Osypowski, Nucl. Phys. **B101**, 136 (1975); E. T. Osypowski, *ibid.* **B21**, 615 (1970).
- [34] T. Sasakawa and S. Ishikawa, Few-Body Syst. **1**, 3 (1986).
- [35] S. Ishikawa, Few-Body Syst. **32**, 229 (2003).
- [36] S. Ishikawa, Few-Body Syst. **40**, 145 (2007).
- [37] K. Sagara, H. Oguri, S. Shimizu, K. Maeda, H. Nakamura, T. Nakashima, and S. Morinobu, Phys. Rev. C **50**, 576 (1994).
- [38] S. Shimizu, K. Sagara, H. Nakamura, K. Maeda, T. Miwa, N. Nishimori, S. Ueno, T. Nakashima, and S. Morinobu, Phys. Rev. C **52**, 1193 (1995).
- [39] S. Ishikawa, M. Tanifuji, and Y. Iseri, Phys. Rev. C **67**, 061001(R) (2003).
- [40] S. Ishikawa, M. Tanifuji, and Y. Iseri, in *Proceedings of the Seventeenth International IUPAP Conference on Few-Body Problems in Physics, Durham, North Carolina, USA, 2003*, edited by W. Glöckle and W. Tornow, (Elsevier, Amsterdam, 2004), p. S61.
- [41] K. Hatanaka, N. Matsuoka, H. Sakai, T. Saito, K. Hosono, Y. Koike, M. Kondo, K. Imai, H. Shimizu, T. Ichihara, K. Nisimura, and A. Okihana, Nucl. Phys. **A426**, 77 (1984).
- [42] M. R. Robilotta, Phys. Rev. C **74**, 044002 (2006).
- [43] V. Bernard, N. Kaiser, J. Kambor, and U.-G. Meissner, Nucl. Phys. **B388**, 315 (1992).